


Large-scale demixing in a binary mixture of cells with rigidity disparity in biological tissuesBao-quan Ai * and Rui-xue Guo*Guangdong Provincial Key Laboratory of Quantum Engineering and Quantum Materials, School of Physics and Telecommunication Engineering, South China Normal University, Guangzhou 510006, China
and Guangdong-Hong Kong Joint Laboratory of Quantum Matter, South China Normal University, Guangzhou 510006, China*

(Received 18 July 2021; revised 3 October 2021; accepted 15 December 2021; published 30 December 2021)

Physical demixing on large scales of embryonic cell populations is fundamental to metazoan development, but whether a rigidity disparity alone is sufficient to driving large-scale demixing in a binary mixture of cell tissues is still an open question. To answer this question, we study mixing and demixing in a binary mixture of rigidity disparity cell tissues without heterotypic interactions using the Voronoi-based cellular model. Under suitable system parameters, the solid-like cells in the mixture can aggregate into a large cluster and the large-scale demixing occurs, which addresses that a rigidity disparity alone is sufficient to drive large-scale demixing. Remarkably, there exists an optimal temperature or rigidity disparity at which the binary mixture can be separated to the maximum extent. The necessary condition for the separation of mixtures is that the two types of cells are solid-like and liquid-like, respectively. The observation of robust demixing on large scales suggests that the sorting of progenitor cells may occur very early in the development process before robust heterotypic interfacial tensions are established. Our findings are relevant to understanding the mechanisms that drive cell sorting in confluent tissues.

DOI: [10.1103/PhysRevE.104.064411](https://doi.org/10.1103/PhysRevE.104.064411)**I. INTRODUCTION**

Soft matter systems are usually multicomponent, consisting of distinct species that are either mixed or demixed, depending on the system parameters. Particles with different properties (mass, size, motility, chirality, etc.) can be separated in different systems [1–25]. Examples include mixtures of active particles with different properties [1–5], chiral active particles [6–10], and active and passive Brownian particles [11–14]. The mixture and separation of each particle type give rise to an exceedingly rich phenomenology compared to monodisperse systems.

Recently, there has been an increasing interest in cell sorting in biological tissues [26–28]. Separation at the subcellular level can lead to compartmentalization within cells [28], while in a developing organism, demixing can lead to cell sorting. Physical separation of embryonic cell populations is fundamental to metazoan development. Recently, from *in vitro* experiments and cellular Potts model simulations, Canty and coworkers [26] found that ephrin-Eph-based repulsion is very effective at inducing and maintaining separation, whereas differences in adhesion or contractility have surprisingly little impact, showing that a large heterotypic line tension between tissues is key to their segregation. To explore the possibility of interfacial-tension-driven demixing in the absence of explicit heterotypic line tension, Sahu and coworkers [27] studied whether a disparity in cell shape or size alone is sufficient to drive demixing in bidisperse vertex model fluid mixtures. They observed large-scale mixing and small-scale demixing

in mixtures with differential adhesion. However, in this work, both rigidity disparity and temperature are small. Therefore, whether the mixed cells without heterotypic interactions in biological tissues can be separated on a large scale is still an open question.

To answer this open question, we studied the mixing behavior of bidisperse cell mixture based on Voronoi-based cellular model in the absence of heterotypic interactions. From numerical simulations, we find that the solid-like cells in the mixture can aggregate into a large cluster under the suitable system parameters, which indicates that the mixed cells without heterotypic interactions in biological tissues can spontaneously demix on large scales. Therefore, a rigidity disparity alone is sufficient to drive large-scale demixing in a binary mixture of cell tissues. The optimum temperature or rigidity disparity results in the maximum separation of the binary mixture. The necessary condition for the separation of mixtures is that the two types of cells are solid-like and liquid-like, respectively. The separation behavior is almost independent of the size of the system. The robustness of large-scale demixing suggests that the sorting of progenitor cells may occur very early in the development process before robust heterotypic interfacial tensions are established.

II. MODEL AND METHODS

Simple models that represent cells as polygons have been successful in describing both the static and dynamic aspects of an epithelial monolayer [29–44]. To understand the mechanisms of cell sorting in confluent tissues, we study the binary mixture of cells with rigidity disparity using the Voronoi-based cellular model [29,30] in the absence of the explicit

*aibq@scnu.edu.cn

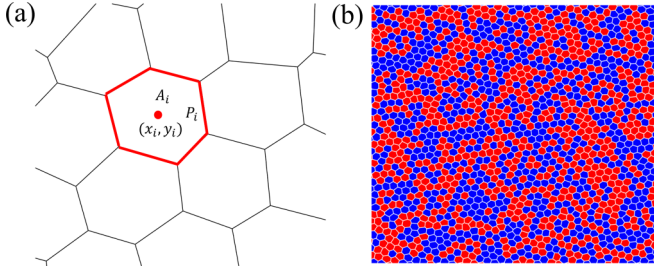


FIG. 1. (a) Schematic of Voronoi-based modeling of a tissue: all forces are applied directly to the center of cells. Only the cell centers are updated and the cell shape is determined by the resulting Voronoi tessellation. The energy from Eq. (1) depends only on a cell's perimeter (P_i) and area (A_i). (b) A typical snapshot of a confluent tissue containing $N/2$ type A cells (blue polygons) and $N/2$ type B cells (red polygons) in a square box of side L with periodic boundary conditions at $p_0 = 3.813$, $\Delta = 1.5$, and $T = 0.0$. The shape indexes for type A and B cells are $p_A = p_0 - \Delta/2$ and $p_B = p_0 + \Delta/2$, respectively. Relatively, type A cells are harder and type B cells are softer.

heterotypic line tension. In contrast to particle-based models, cells in the Voronoi-based cellular model are confluent and can change their shape to completely fill space, thus their interaction is shaped based. The Voronoi model describes a confluent tissue as a network of polygons. Each cell is characterized by its position $\mathbf{r}_i \equiv (x_i, y_i)$, and cell shape is determined by the resulting Voronoi tessellation (shown in Fig. 1). The tissue forces are obtained from an effective energy functional $E(\{\mathbf{r}_i\})$ without heterotypic interactions for N cells, given by [45]

$$E = \sum_{i=1}^N [K_a(A_i - A_{0,i})^2 + K_p(P_i - P_{0,i})^2], \quad (1)$$

where A_i and P_i are the cross-sectional area and perimeter of the i th cell. $A_{0,i}$ and $P_{0,i}$ are the preferred cell area and perimeter for cell i . K_a and K_p represent the area and perimeter stiffness moduli, respectively. The first term models cell incompressibility and the monolayer's resistance to height fluctuations. The second term arises from active contractility of the actomyosin subcellular cortex and effective cell membrane tension due to cell-cell adhesion and cortical tension. For convenience, we assume that the preferred cell area $A_{0,i}$ does not vary and is set to be A_0 . The effective dimensionless target shape index $p_{0,i} = P_{0,i}/\sqrt{A_0}$ is an important parameter that controls the elastic behavior of the cells. Geometrically, a regular pentagon corresponds to $p_{0,i} \approx 3.81$ and a regular hexagon to $p_{0,i} \approx 3.72$.

In this study, we consider a binary mixture of $N/2$ cells with the shape index p_A (named type A cells) and $N/2$ cells with the shape index p_B (named type B cells) in a square box of side $L (= \sqrt{NA_0})$ with periodic boundary conditions (shown in Fig. 1). The average shape index is $p_0 = (p_A + p_B)/2$ and the rigidity disparity is described by $\Delta p = p_B - p_A$ with $p_B > p_A$. From the expression for the elastic energy in Eq. (1), we can see that the system softens when the target shape index increases. When $p_0 < p_0^*$ (the critical value p_0 at the rigidity transition), cortical tension dominates over cell-

cell adhesion and the tissue behaves as an elastic solid. When $p_0 > p_0^*$, cell-cell adhesion dominates and the energy barriers for local rearrangements vanish, resulting in zero rigidity and fluid-like behavior. Therefore, one naturally expects a solid phase with small shape index, and a liquid phase with large shape index.

The effective energy of Eq. (1) leads to a mechanical interaction force on cell i by $F_i = -\nabla_i E$ (see the Supplemental Material [46]). In contrast to particle-based models, F_i is a multibody interaction force that cannot be expressed as a sum of the pairwise force between cell i and its neighboring cells. To simulate the dynamics of the model, each cell undergoes overdamped Brownian motion at a given temperature. Thus, the dynamic of cell i in the overdamped limit follows the Langevin equation

$$\frac{d\mathbf{r}_i}{dt} = \mu F_i + \sqrt{2D}\xi_i(t), \quad (2)$$

where $\xi_i(t)$ are Gaussian white noises with zero mean and unit variance. The thermal diffusion coefficient D and the mobility μ fulfill the Einstein relation $D = \mu k_B T$, where T the temperature and k_B is the Boltzmann constant.

Equations (1) and (2) can be rewritten in the dimensionless forms by introducing the characteristic length $\sqrt{A_0}$ and time $1/(\mu K_a A_0)$. The parameters in the dimensionless forms can be rewritten as $\hat{K}_p = K_p/(K_a A_0)$, $\hat{L} = L/\sqrt{A_0} = \sqrt{N}$, and $\hat{T} = \frac{k_B T}{K_a A_0}$. From now on, we will use only the dimensionless variables and shall omit the hat for all quantities occurring in the above equations.

To quantify the spatial distribution of cell types A and B, we divide the area $L \times L$ into M square subregions, the segregation coefficient S is given by

$$S = \frac{1}{N} \sum_j^M |N_j^A - N_j^B|, \quad (3)$$

where N_j^A and N_j^B are the number of cell types A and B in the j th subregion, respectively. With this definition, the binary mixture is completely mixed when $S = 0$ and completely demixed when $S = 1$. Note that to calculate the segregation coefficient S , M must not be too large or too small. Although the segregation coefficient S is related to M , S still can well describe the separation state of the mixture if we choose a reasonable M (see the Supplemental Material [46]).

To study the dynamics behavior of the system, we use the mean square displacement (MSD), $\text{MSD}(t) = \langle [r(t + t_0) - r(t_0)]^2 \rangle$, where $\langle \dots \rangle$ denotes an average over all time t_0 and all cells in the tissue. The normalized self-diffusivity D_{eff} is obtained by assuming the long-time behavior $D_{\text{eff}} = \lim_{t \rightarrow \infty} \frac{\text{MSD}(t)}{4tD}$. The system is solid-like for small D_{eff} and fluid-like for large D_{eff} . Therefore, the normalized self-diffusivity can be used as an accurate dynamical order parameter that distinguishes a fluid state from a solid state.

We use the relative radial distribution function to describe the characteristic cluster size of the single cell species in the binary mixtures. For two cell types A and B, their densities are $\rho_A(\mathbf{r}) = \sum_{i=1}^{N_A} \delta(\mathbf{r} - \mathbf{r}_i)$ and $\rho_B(\mathbf{r}) = \sum_{i=1}^{N_B} \delta(\mathbf{r} - \mathbf{r}_i)$, respectively. We define the relative radial distribution function for

the binary mixture as the autocorrelation function [8,18]

$$\begin{aligned}
 g_{AB}(\mathbf{r}_1, \mathbf{r}_2) &= \langle \rho_{AB}(\mathbf{r}_1) \rho_{AB}(\mathbf{r}_2) \rangle \\
 &= \langle \rho_A(\mathbf{r}_1) \rho_A(\mathbf{r}_2) \rangle + \langle \rho_B(\mathbf{r}_1) \rho_B(\mathbf{r}_2) \rangle \\
 &\quad - \langle \rho_A(\mathbf{r}_1) \rho_B(\mathbf{r}_2) \rangle - \langle \rho_B(\mathbf{r}_1) \rho_A(\mathbf{r}_2) \rangle, \quad (4)
 \end{aligned}$$

where $\rho_{AB}(\mathbf{r}) = \rho_A(\mathbf{r}) - \rho_B(\mathbf{r})$. In the homogeneous and isotropic systems, Eq. (4) reduces to $g_{AB}(r)$ with $r = |\mathbf{r}_1 - \mathbf{r}_2|$. $g_{AB}(r)$ is negative if at distance r mainly cells of the different species contribute to the average and positive if mainly cells from equal species contribute to the average. The roots of $g_{AB}(r)$ are found at distances, where cell types A and B appear with equal probability. The characteristic cluster size is determined by the first nontrivial root of $g_{AB}(r)$ [8,18].

In our simulations, all forces are applied directly to the center of cells. At every time step, only the cell centers are updated and a new Voronoi tessellation is obtained from the updated cell centers. The intercellular forces are then calculated based on shapes and topologies of the Voronoi cells (see the Supplemental Material [46]). Equation (2) is numerically integrated using a stochastic Runge-Kutta algorithm. The integration time step was chosen to be 0.001 and the total integration time was more than 2×10^5 (this time is sufficient to ensure that the system can reach a steady state). For all simulation runs, we start with a set of N random cell positions (the two type cells are uniformly distributed in the initial state) and wait for equilibration before recording data. We considered 100 realizations to improve the accuracy and minimize statistical errors. Unless otherwise noted, we set $K_p = 1$, $N = 1600$, and $M = 10 \times 10 = 100$ throughout the simulations. We tested that the presented results are robust against reasonable changes in these parameters.

III. RESULTS AND DISCUSSION

To study whether a rigidity disparity alone is sufficient to drive large-scale demixing, we explore the demixing behavior in a binary mixture of cell tissues by varying the temperature T , the average shape index p_0 , and the rigidity disparity Δ .

We discuss the demixing mechanism of the mixed cells, three typical cases are shown in Fig. 2. When a cell is trying to squeeze through two cells of different type, whether or not this cell can squeeze through two cells of different type, we cannot judge whether the mixture can be separated. Therefore, we only consider the case of a single cell squeezing through two homotypic cells with the opposite cell type. For case I, the two types of cells can easily squeeze through each other, once a cluster of type A (B) cells forms, it is quickly destroyed by type B (A) cells, the two types of cells cannot aggregate separately, so the mixture is mixed. For case II, type A cells can easily squeeze through two type B cells, but type B cells cannot squeeze through two type A cells, once two type A cells meet, they will be connected. In this case, type A cells keep aggregating and finally form a large cluster, thus the mixture of two types of cells can be separated. For case III, the two types of cells cannot squeeze through each other, both type A and B cells cannot aggregate into clusters, so the mixture cannot be separated. Therefore, only in case II, the demixing of the binary mixing system is possible. To satisfy case II, a

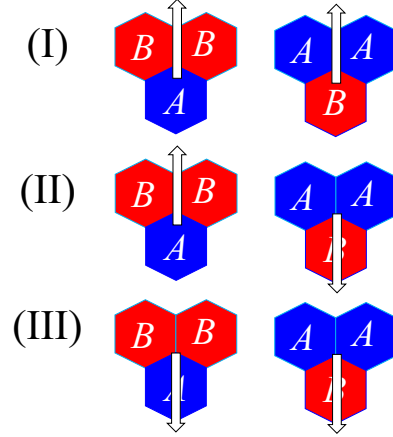


FIG. 2. The illustrative sketches for the interactions between two mixed cells. (i) The two types of cells can easily squeeze through each other and the mixture cannot be separated. (ii) Type A cells can easily squeeze through two type B cells, but type B cells cannot cross through two type A cells. In this case, type A cells will aggregate into a large cluster and the mixture is demixed. (iii) The two types of cells cannot squeeze through each other and the system is mixed.

significant difference between two types of cells and a driving force (e.g., Brownian motion) are required.

We first study how the rigidity disparity Δ affects the fluidity of the tissue by using the normalized self-diffusivity D_{eff} . We consider the case of $p_0 = 3.813$, where a rigidity transition occurs [30–32] for the monodisperse system at zero temperature. Here we used a threshold of $D_{\text{eff}} = 0.01$ to distinguish between a liquid state and a solid state. As an example, the normalized self-diffusivity D_{eff} as a function of Δ is shown in Fig. 3 for different cases at $T = 0.02$. In this case, the system behaves as a liquid state at $\Delta = 0$. It is found that each single cell type exhibits the different behaviors in the presence or not of another cell type. In the monodisperse

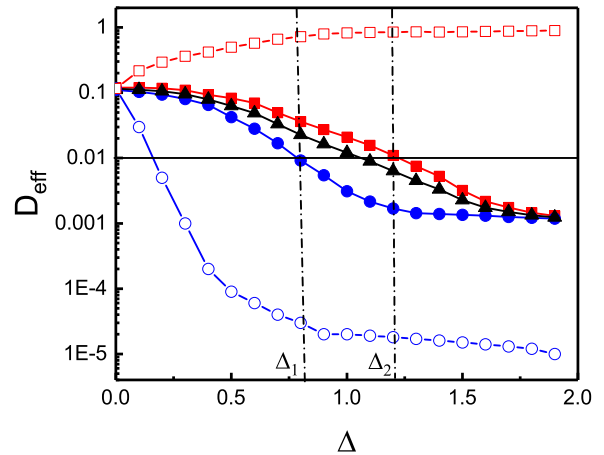


FIG. 3. The normalized self-diffusivity D_{eff} as a function of Δ at $p_0 = 3.813$ and $T = 0.02$ for different cases: type A cells in the mixture (solid circles), type B cells in the mixture (solid squares), the whole mixture (solid triangles), type A cells in the monodisperse system (hollow circles), and type B cells in the monodisperse system (hollow squares).

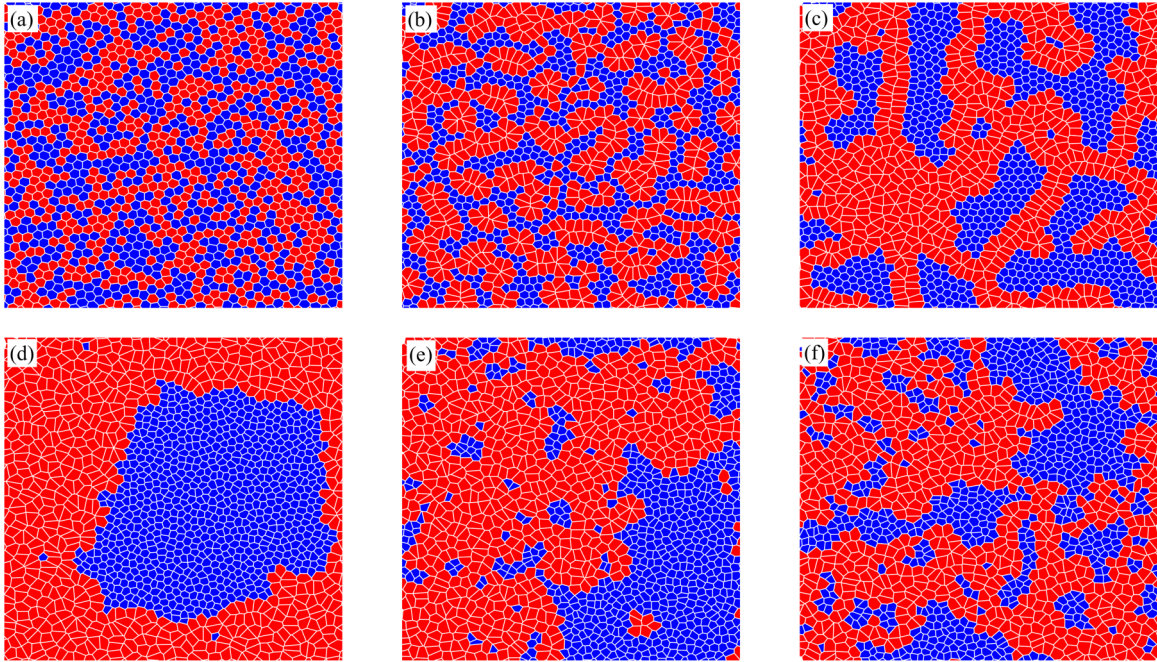


FIG. 4. Typical snapshots of the binary system of 800 type *A* cells (blue polygons) and 800 type *B* cells (red polygons) for different temperature at $p_0 = 3.813$ and $\Delta = 1.5$. (a) $T = 0.0$. (b) $T = 0.005$. (c) $T = 0.02$. (d) $T = 0.03$. (e) $T = 0.08$. (f) $T = 0.095$.

system, D_{eff} increases with Δ for type *B* cells and decreases with the increase of Δ for type *A* cells. However, in the binary system, the normalized self-diffusivity D_{eff} decreases with the increase of Δ for all cases, which indicates that large rigidity disparity Δ will harden the system. For small Δ , type *B* cells are indeed able to help type *A* cells diffuse. For large Δ , type *A* cells in the mixture are sufficient to freeze the entire tissue. Both types *A* and *B* cells are fluid-like for $\Delta < \Delta_1$ and solid-like for $\Delta > \Delta_2$. Interestingly, when $\Delta_1 < \Delta < \Delta_2$, type *A* cells are solid-like, while type *B* cells are fluid-like, which satisfies the case II in Fig. 2. Note that this interval ($\Delta_1 < \Delta < \Delta_2$) shifts to large Δ when T increases. Figure 4 shows the typical snapshots of the binary system for different T at $p_0 = 3.813$ and $\Delta = 1.5$. When the rigidity disparity Δ is fixed, the demixing behavior of cells is determined by temperature T . At zero temperature [shown in Fig. 4(a)], two types of cells cannot squeeze through each other, which is the case III in Fig. 2, so the system is mixed. At low temperature [e.g., $T = 0.005$ in Fig. 4(b)], a few type *A* cells squeeze through two type *B* cells and aggregate into some small clusters, but MSD for both components in the mixture tends to be saturated with time (shown in Fig. 5), which shows that both types *A* and *B* cells are solid-like. As temperature T increases, type *A* cell cluster gradually grows larger [shown in Fig. 4(c)]. Remarkably, at $T = 0.03$, MSD (shown in Fig. 5) tends to be saturated with time for type *A* cells and increases linearly with time for type *B* cells, which shows that type *A* cells are solid-like and type *B* cells are fluid-like. In this case, type *A* (solid-like) cells can swim through type *B* (liquid-like) cells, all type *A* cells aggregate into a large cluster [shown in Fig. 4(d)] which corresponds to the case II in Fig. 2, so the mixture of two types of cells can be completely separated. On further increasing T due to strong Brownian motion, a few type *B* cells squeeze through two type *A* cells, so the big

type *A* cell cluster is gradually destroyed [shown in Fig. 4(e)]. When the temperature is high (e.g., $T = 0.095$), MSD (shown in Fig. 5) increases linearly with time for both types *A* and *B* cells, which shows that two components are fluid-like. In this case, the two types of cells can easily squeeze through each other, the mixture is mixed, which corresponds to the case I in Fig. 2. Therefore, when fixing the rigidity disparity Δ , there exists an optimal value of temperature T at which two types of cells are completely demixed, which addresses that a rigidity disparity alone is sufficient to drive large-scale demixing.

In Fig. 6, we plotted the relative radial distribution function $g_{AB}(r)$ for different T at $p_0 = 3.813$ and $\Delta = 1.5$. The cluster size of the single cell specie is determined by the first

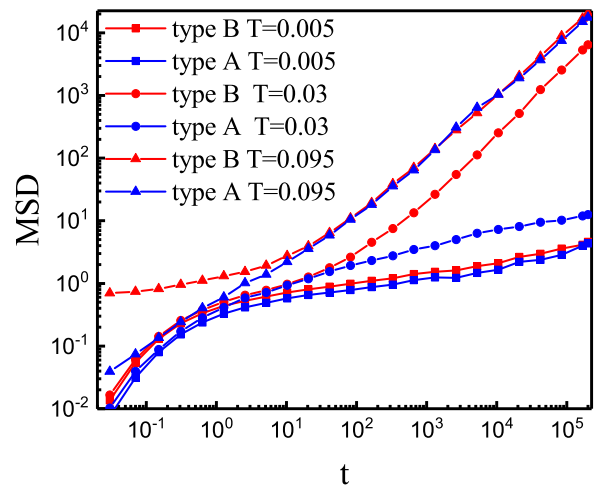


FIG. 5. MSD for different components and different T at $p_0 = 3.813$.

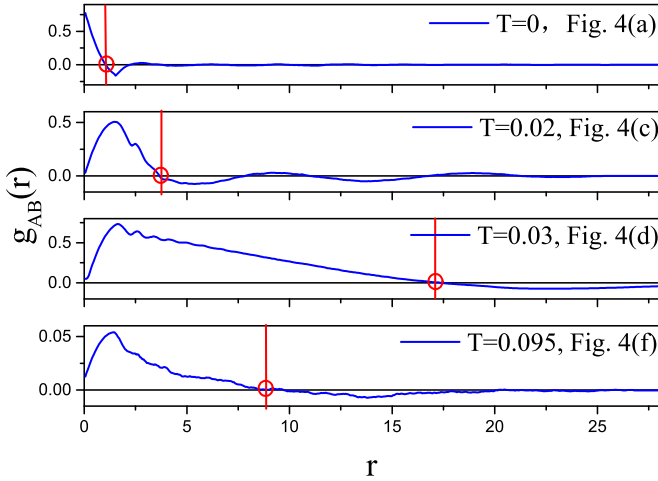


FIG. 6. Relative radial distribution function $g_{AB}(r)$ at $t = 2 \times 10^5$ for $T = 0, 0.02, 0.03,$ and 0.095 , which corresponds to Figs. 4(a), 4(c), 4(d), and 4(f), respectively. The first nontrivial root (marked by circles) is a quantifier for the cluster size of the single particle species.

nontrivial zero of $g_{AB}(r)$ (marked by red circles). It is found that when T increases from 0, the cluster size first increases to the maximum and then decreases gradually. Specifically, the cluster size of the single cell species is very large at $T = 0.03$. The cluster size is very small at $T = 0$, which means that the mixture is mixed.

We use the separation coefficient S defined in Eq. (3) to describe the degree of separation of binary mixtures. The segregation coefficient S as a function of temperature T is shown in Fig. 7(a) for different Δ at $p_0 = 3.813$. The segregation coefficient S is a peaked function of temperature T . When $T \rightarrow 0$, two types of cells cannot squeeze through each other, the system is mixed, so S is small. When T is very large, the two types of cells can easily squeeze through each other, thus the mixture is also mixed. Therefore, there exists an optimal temperature T at which S takes its maximal value. In addition, the position of the peak shifts to large T with the increase of Δ . This can be explained as follows. The peak in the curves

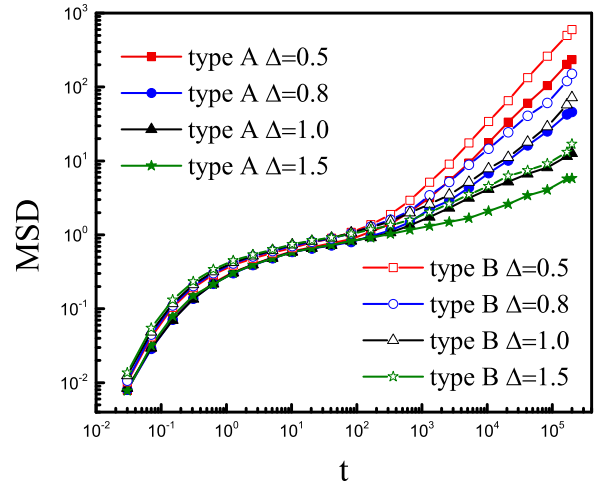


FIG. 8. MSD of two types of cells in the mixture for different Δ at $T = 0.01$ and $p_0 = 3.813$. MSD of two types of cells decreases with the increase of Δ .

means that type B cells start to cross through type A cells. As Δ increases, the MSD of type A cells (shown in Fig. 8) decreases, which means that type A cells become harder, so type B cells need a higher temperature to swim through two type A cells.

The dependence of the segregation coefficient S on the rigidity disparity Δ is shown in Fig. 7(b) for different T at $p_0 = 3.813$. When $\Delta \rightarrow 0$, the two types of cells are almost identical and cannot be separated, so S is very small. From Fig. 3, we can find that there exists an interval ($\Delta_1 < \Delta < \Delta_2$), where type A cells are solid-like, while type B cells are fluid-like. In this regime, type A cells can easily squeeze through two type B cells, but type B cells cannot cross through two type A cells, type A cells keep aggregating and finally form a large cluster, thus the mixture of two types of cells can easily be separated. When Δ is very large, both types A and B cells are solid-like (very small D_{eff} shown in Fig. 3). In this case, the two types of cells cannot squeeze through each other, so the mixture is mixed. Therefore, at the finite temperature, there exists an optimal value of Δ at which the segregation

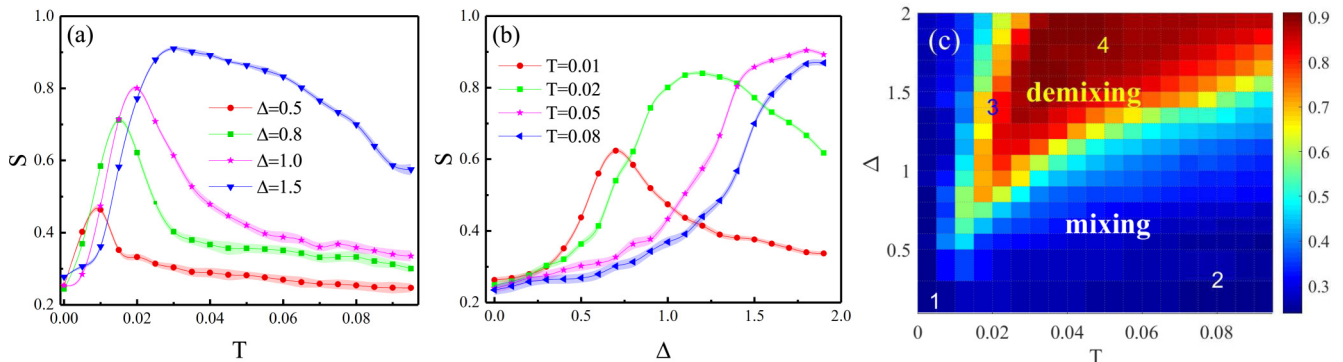


FIG. 7. (a) Segregation coefficient S as a function of temperature T for different rigidity disparity Δ at $p_0 = 3.813$. (b) Segregation coefficient S as a function of the rigidity disparity Δ for temperature T at $p_0 = 3.813$. The solid line is the average over 100 independent simulations and the shaded region shows standard deviation above and below the average. (c) Phase diagram of the binary mixtures in the $T - \Delta$ representation with $p_0 = 3.813$. The four points (1–4) in the figure correspond to Figs. 9(a)–9(d). The background represents the value of S according to the color bar on the right.

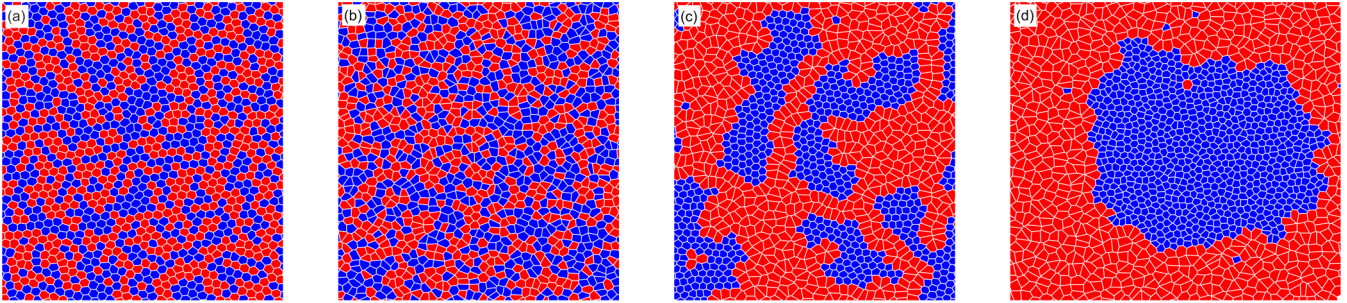


FIG. 9. Typical snapshots for different points in Fig. 7(c). (a) $\Delta = 0.0$ and $T = 0.005$. (b) $\Delta = 0.3$ and $T = 0.08$. (c) $\Delta = 1.4$ and $T = 0.02$. (d) $\Delta = 1.8$ and $T = 0.05$. Figures (a)–(d) correspond to points 1–4 in Fig. 7(c), respectively.

coefficient S is maximal. Larger rigidity disparity Δ does not mean the larger separation coefficient S . Additionally, the position of the peak in the curves shifts to large Δ as T increases.

To study in more detail the dependence of the segregation coefficient S on temperature T and the rigidity disparity Δ , we plotted the phase diagram of the binary mixtures in the $T - \Delta$ representation at $p_0 = 3.813$ in Fig. 7(c). The typical snapshots are shown in Fig. 9 for different regions (points 1–4) in Fig. 7(c). Both mixing and demixing regions are clearly shown in the diagram. When $\Delta < 0.5$ or $T < 0.01$, the segregation coefficient S is small and the mixture cannot be separated, which indicates that large rigidity disparity and strong thermal movement are two important conditions for cell separation. However, high temperature and large rigidity disparity are not always conducive to cell separation. There exists the appropriate parameter region where the mixture can be separated. When p_0 decreases from 3.813, the demixing zone in the diagram will shrink. However, the demixing zone will expand and shift to small rigidity disparity and low temperature when p_0 increases from 3.813. Note that this phase diagram does not change qualitatively when the other parameters are varied.

We discuss the role of the average shape index p_0 in the separation of mixtures. The segregation coefficient S as a function of p_0 is shown in Fig. 10(a) for two cases. It is found that the segregation coefficient S increases with p_0 for two cases. Since $p_A = p_0 - \Delta/2$ and $p_B = p_0 + \Delta/2$, both p_A and p_B increases with p_0 [shown in Fig. 10(b)]. The shape index p_A (for type A cells) for two cases is always smaller than 3.813, so type A cells are always solid-like. However, type B cells are solid-like when $p_0 < 3.315$ (3.063) and liquid-like when $p_0 > 3.315$ (3.063) at $\Delta = 1.0$ (1.5). Obviously, the mixture can be separated only when type A cells are solid-like and type B cells are liquid-like. Therefore, it is impossible to separate the mixture when $p_0 < 3.315$ (3.063) at $\Delta = 1.0$ (1.5). Increasing p_0 from 3.0, type B cells gradually changed from solid-like cells to liquid-like cells, so the segregation coefficient S increases. Therefore, the two types of cells are solid-like and liquid-like, respectively, which is the necessary condition for the separation of mixtures.

We study the effect of the system size on demixing of the mixture, the segregation coefficient S versus the total cell number N is described in Fig. 11 for two cases. Since S depends on M , to compare the segregation coefficient S for different system size N , we fixed $N/M = 16$ for all cases. It

should be noted that for large system size, it takes a long time for the system to reach equilibrium. We find no significant change in the separation coefficient S when the system size N changes, which indicates that the demixing in the mixed cell tissues is not a finite size effect.

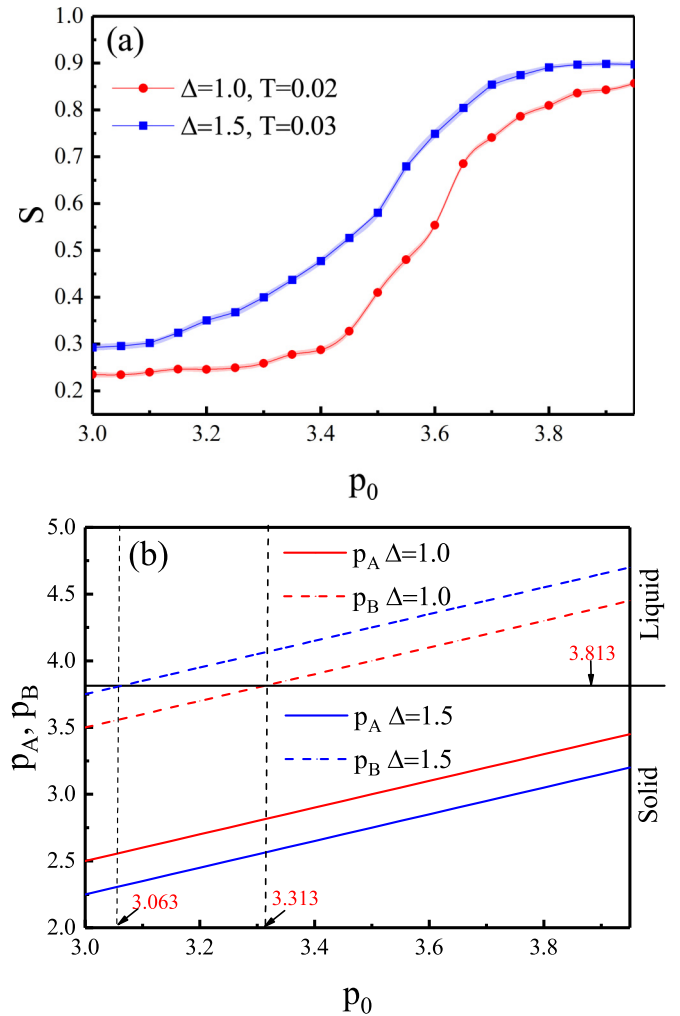


FIG. 10. (a) Segregation coefficient S as a function of the average shape index p_0 for different cases. (b) Shape indexes p_A and p_B as a function of the average shape index p_0 for $\Delta = 1.0$ and 1.5. $p_A = p_0 - \Delta/2$ and $p_B = p_0 + \Delta/2$. The black solid line represents the shape index (3.813) of the rigid transition at zero temperature.

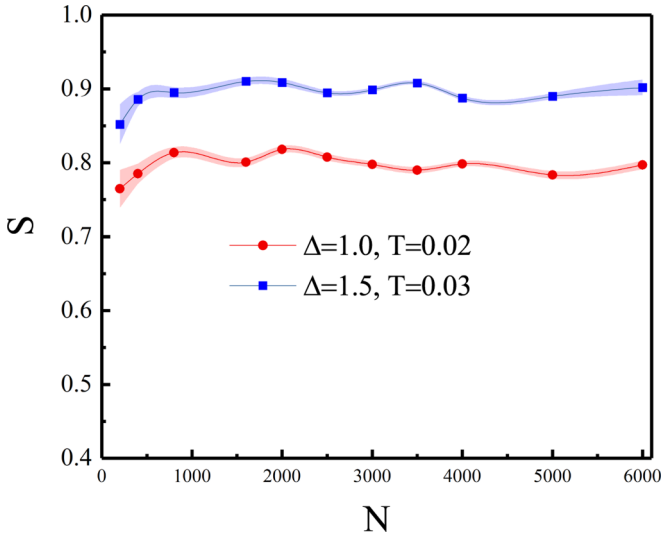


FIG. 11. Segregation coefficient S as a function of the total cell number N for different cases at $p_0 = 3.813$. We demonstrate the absence of finite size effects, showing the segregation coefficient S is obtained irrespective of system size N .

Finally, we discuss the possibility of realizing our model in the experiment setups. The experiment proposed by Sahu and coworkers [27] is very convenient to determine whether or not large-scale demixing prediction is directly relevant for biology. In the experiment, bidisperse cell mixture is consist of both wild-type keratinocytes and E-cadherin-knock-out keratinocytes, which allows us to study differential adhesion and its effect on cell sorting without heterotypic tensions. Because E-cadherin is a crucial component of adherens junctions, E-cadherin-knock-out keratinocytes (primary keratinocytes in which the E-cadherin has been knocked down) are softer than wild-type keratinocytes. Therefore, there exists a rigidity disparity in the two-component mixture. Wild-type keratinocytes and E-cadherin-knock-out keratinocytes correspond to type A and B cells in the model, respectively. First, it is necessary to obtain the mixture with large rigidity disparity, which may be achieved by changing the experimental conditions (e.g., temperature, calcium concentration, the persistent motion of cells, differential mechanical stiffness of the cells, etc.). Next, a large number of snapshots of the monolayer need to be obtained in the experiment. From the snapshots, we can calculate the segregation coefficient for different cases. Additionally, the sorting mechanism in our model might happen in an embryo. For example, we can hold an embryo to a constant dose of an inhibitor (Latrunculin, cytochalasin, or blebbistatin) of the actin cytoskeleton [47]. The inhibitors inhibit the role of the actin cytoskeleton which can determine

the stiffness of a cell along with the microtubules [48,49]. Therefore, we can obtain the mixed cells with rigidity disparity by adjusting the dose or type of inhibitors. We hope to observe large-scale demixing in these experiments.

IV. CONCLUSION AND OUTLOOK

By using the Voronoi-based cellular model, we studied mixing and demixing in a binary mixture of rigidity disparity cell tissues in the absence of the explicit heterotypic line tension. When the average shape index p_0 is fixed, the demixing behavior of the bidisperse cell mixture is determined by the rigidity disparity Δ and temperature T . When T (or Δ) is too small or too large the segregation coefficient S is small and the mixture cannot be separated. There exists the optimal T or Δ at which the segregation coefficient S is maximal and the mixture can be separated. Specifically, the greater the difference of the cell rigidity does not mean that the mixture is easier to separate. Therefore, we observed large-scale demixing under suitable system parameters, which shows that a rigidity disparity alone is sufficient to drive large-scale demixing. Only when the two kinds of cells are solid-like and liquid-like, respectively, may the mixture be separated. There is no significant change in the separation coefficient S when the system size N changes. Our results on the one hand suggests that the sorting of progenitor cells may occur very early in the development process before robust heterotypic interfacial tensions are established. On the other hand, our results also confirm the possibility of large-scale demixing in the confluent systems, where the interactions between particles are multibody and the particles can change their shape to completely fill space (the packing fraction is precisely at unity). We hope that our results can be realized in the experiments of binary mixtures, for example, mixtures of wild-type and E-cadherin-deficient keratinocytes [27]. Finally, our research could have potential applications in biological processes including embryonic development, cancer metastasis, and wound healing require cells to move collectively in dense tissues, which is very different from isolated cell motion.

ACKNOWLEDGMENTS

This work was supported, in part, by the National Natural Science Foundation of China (Grant No. 12075090), the Key-Area Research and Development Program of Guangdong Province (Grant No. 2019B030330001), the Science and Technology Program of Guangzhou (Grant No. 2019050001), the Natural Science Foundation of Guangdong Province (Grant No. 2017A030313029), and the Major Basic Research Project of Guangdong Province (Grant No. 2017KZDXM024).

- [1] C. Maggi, A. Lepore, J. Solari, A. Rizzo, and R. Di Leonardo, *Soft Matter* **9**, 10885 (2013).
- [2] W. Yang, V. R. Misko, K. Nelissen, M. Kong, and F. M. Peeters, *Soft Matter* **8**, 5175 (2012).
- [3] I. Berdakin, Y. Jeyaram, V. V. Moshchalkov, L. Venken, S. Dierckx, S. J. Vanderleyden, A. V. Silhanek, C. A. Condat, and V. I. Marconi, *Phys. Rev. E* **87**, 052702 (2013).

- [4] S. N. Weber, C. A. Weber, and E. Frey, *Phys. Rev. Lett.* **116**, 058301 (2016).
- [5] S. Kumari, A. S. Nunes, N. A. M. Araujo, and M. M. T. Gama, *J. Chem. Phys.* **147**, 174702 (2017).
- [6] M. Mijalkov and G. Volpe, *Soft Matter* **9**, 6376 (2013).
- [7] C. Reichhardt and C. J. Olson Reichhardt, *Phys. Rev. E* **88**, 042306 (2013).

- [8] C. Scholz, M. Engel, and T. Pöschel, *Nat. Commun.* **9**, 931 (2018).
- [9] Q. Chen and B. Q. Ai, *J. Chem. Phys.* **143**, 104113 (2015).
- [10] B. Q. Ai, Z. G. Shao, and W. R. Zhong, *Soft Matter* **14**, 4388 (2018).
- [11] S. R. McCandlish, A. Baskarana, and M. F. Hagan, *Soft Matter* **8**, 2527 (2012).
- [12] J. Stenhammar, R. Wittkowski, D. Marenduzzo, and M. E. Cates, *Phys. Rev. Lett.* **114**, 018301 (2015).
- [13] Z. Ma, Q. Lei, and R. Ni, *Soft Matter* **13**, 8940 (2017).
- [14] J. Smrek and K. Kremer, *Phys. Rev. Lett.* **118**, 098002 (2017).
- [15] J. Harder and A. Cacciuto, *Phys. Rev. E* **97**, 022603 (2018).
- [16] A. Costanzo, J. Elgeti, T. Auth, G. Gompper, and M. Ripoll, *Europhys. Lett.* **107**, 36003 (2014).
- [17] A. Nourhani, V. H. Crespi, and P. E. Lammert, *Phys. Rev. Lett.* **115**, 118101 (2015).
- [18] N. H. P. Nguyen, D. Klotsa, M. Engel, and S. C. Glotzer, *Phys. Rev. Lett.* **112**, 075701 (2014).
- [19] A. Agrawal and S. B. Babu, *Phys. Rev. E* **97**, 020401(R) (2018).
- [20] B. Q. Ai, Y. F. He, and W. R. Zhong, *Soft Matter* **11**, 3852 (2015).
- [21] B. Q. Ai, B. Y. Zhou, and X. M. Zhang, *Soft Matter* **16**, 4710 (2020).
- [22] J. Shin, A. G. Cherstvy, and R. Metzler, *New J. Phys.* **16**, 053047 (2014).
- [23] D. Levis and B. Liebchen, *Phys. Rev. E* **100**, 012406 (2019).
- [24] P. Dolai, A. Simha, and S. Mishrac, *Soft Matter* **14**, 6137 (2018).
- [25] A. Wysocki, R. G. Winkler, and G. Gompper, *New J. Phys.* **18**, 123030 (2016).
- [26] L. Canty, E. Zarour, L. Kashkooli, P. Francois, and F. Fagotto, *Nat. Commun.* **8**, 157 (2017).
- [27] P. Sahu, D. M. Sussman, M. Rubsam, A. F. Mertz, V. Horsley, E. R. Dufresne, C. M. Niessen, M. Cristina Marchetti, M. L. Manning, and J. M. Schwarz, *Soft Matter* **16**, 3325 (2020).
- [28] M. Feric, N. Vaidya, T. S. Harmon, D. M. Mitrea, L. Zhu, T. M. Richardson, R. W. Kriwacki, R. V. Pappu, and C. P. Brangwynne, *Cell* **165**, 1686 (2016).
- [29] X. Yang, D. Bi, M. Czajkowskic, M. Merkel, M. Lisa Manning, and M. C. Marchetti, *Proc. Natl. Acad. Sci. USA* **114**, 12663 (2017).
- [30] Y. W. Li and M. P. Ciamarra, *Phys. Rev. Materials* **2**, 045602 (2018).
- [31] D. Bi, J. H. Lopez, J. M. Schwarz, and M. L. Manning, *Nat. Phys.* **11**, 1074 (2015).
- [32] D. Bi, X. Yang, M. C. Marchetti, and M. L. Manning, *Phys. Rev. X* **6**, 021011 (2016).
- [33] X. Li, A. Das, and D. Bi, *Proc. Natl. Acad. Sci. USA* **115**, 6650 (2018).
- [34] L. Yan and D. Bi, *Phys. Rev. X* **9**, 011029 (2019).
- [35] T. Nagai and H. Honda, *Phys. Rev. E* **80**, 061903 (2009).
- [36] X. Trepatt and E. Sahai, *Nat. Phys.* **14**, 671 (2018).
- [37] S. Alt, P. Ganguly, and G. Salbreux, *Phil. Trans. R. Soc. B* **372**, 20150520 (2017).
- [38] D. Barton, S. Henkes, C. Weijer, and R. Sknepnek, *PLoS Comput. Biol.* **13**, e1005569 (2017).
- [39] F. Giavazzi, M. Paoluzzi, M. Macchi, D. Bi, G. Scita, M. L. Manning, R. Cerbino, and M. C. Marchetti, *Soft Matter* **14**, 3471 (2018).
- [40] D. M. Sussman, *Phys. Rev. Res.* **2**, 023417 (2020).
- [41] D. M. Sussman and M. Merkel, *Soft Matter* **14**, 3397 (2018).
- [42] D. M. Sussman, *Comput. Phys. Commun.* **219**, 400 (2017).
- [43] S. Henkes, K. Kostanjevec, J. M. Collinson, R. Sknepnek, and E. Bertin, *Nat. Commun.* **11**, 1405 (2020).
- [44] S. Sadhukhan and S. K. Nandi, bioRxiv: <https://doi.org/10.1101/2021.08.21.457184> (2021).
- [45] N. B. Ouchi, J. A. Glazier, J. Rieu, A. Upadhyaya, and Y. Sawada, *Physica A* **329**, 451 (2003).
- [46] See Supplemental Material at <http://link.aps.org/supplemental/10.1103/PhysRevE.104.064411> for (i) simulation algorithm for the Voronoi model and (ii) segregation coefficient, which includes Refs. [27,32,42].
- [47] H. Y. G. Lim and N. Plachta, *Nat. Rev. Mol. Cell Biol.* **22**, 548 (2021).
- [48] B. Doss, M. Pan, M. Gupta, G. Greci, R. Mege, C. T. Lim, M. P. Sheetz, R. Voituriez, and B. Ladoux, *Proc. Natl. Acad. Sci. USA* **117**, 12817 (2020).
- [49] M. Gupta, B. Doss, C. T. Lim, R. Voituriez, and B. Ladoux, *Cell Adhesion and Migration* **10**, 554 (2016).